

Kinetic Flux Ropes: Bernstein-Greene-Kruskal Modes for the Vlasov-Poisson-Ampère System

C. S. Ng^{1, a)}

Geophysical Institute, University of Alaska Fairbanks, Fairbanks, Alaska 99775, USA

(Dated: 22 November 2021)

Electrostatic structures have been observed in many regions of space plasmas, including the solar wind, the magnetosphere, the auroral acceleration region. One possible theoretical description of some of these structures is the concept of Bernstein-Greene-Kruskal (BGK) modes, which are exact nonlinear steady-state solutions of the Vlasov-Poisson system of equations in collisionless kinetic theory. We generalize exact solutions of two-dimensional BGK modes in a magnetized plasma with finite magnetic field strength [Ng, Bhattacharjee, and Skiff, *Phys. Plasmas* **13**, 055903 (2006)] to cases with azimuthal magnetic fields so that these structures carry electric current as well as steady electric and magnetic fields. Such nonlinear solutions now satisfy exactly the Vlasov-Poisson-Ampère system of equations. Explicit examples with either positive or negative electric potential structure are provided.

PACS numbers: 52.35.Sb, 52.25.Dg, 52.35.Mw, 52.25.Xz

Keywords: BGK modes, Solitons, Plasma kinetic equations, Nonlinear phenomena, Magnetized plasmas

I. INTRODUCTION

High temperature plasmas relevant to fusion experiments, space and astrophysics can be considered as collisionless due to small collision frequency.¹ Consequently, particle distributions in a collisionless plasma often deviate from Maxwellian.^{2–4} Studies of the collisionless Vlasov equation have produced many important insights in kinetic theory, e.g., Landau damping of linear plasma waves,^{5–8} and the existence of exact self-consistent steady-state nonlinear solutions of the Vlasov-Poisson equations known as Bernstein-Greene-Kruskal (BGK) modes in one dimension (1D),⁹ i.e., planar structures. A large number of papers have been written on the subject of BGK modes (too many to be cited here but please refer to an interesting recent review¹⁰), but the vast majority of these works were still within the original 1D framework.

The method of constructing a 1D BGK mode is straightforward, either by specifying the form of the distribution first or the electric potential first, as found in some plasma physics textbooks.^{11–13} However, there has also been considerable interest in BGK modes in higher dimensions, i.e., 2D (long tube structures) or 3D (structures localized in all three dimensions). This is mainly due to the fact that 3D features of solitary wave structures in space-based observations that cannot be explained by 1D BGK modes.^{14–17} For example, Ref. 14 shows that electrostatic solitary waves observed in the auroral ionosphere have electric field components perpendicular to the background magnetic field with comparable magnitude to the parallel component. This is inconsistent with a 1D BGK-like potential, which only has

the parallel component, but consistent with the structure of a single-humped solitary potential that travels past the spacecraft along the magnetic field. Also, there are results from numerical simulations suggesting higher dimensional BGK modes.^{18–20}

One kind of approximate 3D BGK modes has been constructed under the assumption of an infinitely strong background magnetic field.^{21–23} The strong field assumption constrains charged particles to move along magnetic field lines, and thus effectively reduces the problem to 1D. To demonstrate in principle that higher dimensional exact BGK modes can indeed exist, we have constructed exact 3D BGK modes (in the geometry of a localized spherically symmetric potential) by allowing the electron distribution function to depend on the angular momentum for an unmagnetized plasma.²⁴ Another kind of solutions that has greater relevance to space plasmas with finite magnetic field has also been constructed under the 2D geometry with cylindrical symmetry.²⁵ Such solutions satisfy exactly the Vlasov-Poisson-Ampère system of equations with the distribution depending on both the energy and the canonical angular momentum. Indeed a Particle-in-Cell (PIC) simulation has found structures similar to our 2D exact solution.²⁶ To study the stability of such 2D BGK modes, we have also performed 2D PIC simulations,²⁷ which show that they are indeed stable for stronger magnetic field.

Electrostatic structures have long been observed experimentally in both magnetized plasmas,^{28,29} trapped pure electron plasmas,³⁰ and in space-based observations of solitary waves or phase space holes in the magnetosphere and the solar wind.^{31–38} Early numerical simulations have also shown that 1D BGK modes can be formed dynamically via a two-stream instability or nonlinear Landau damping and can be reasonably stable.^{39–47}

Meanwhile, kinetic physics down to small electron scales has increasingly been recognized to play a cen-

^{a)} cng2@alaska.edu; <https://sites.google.com/a/alaska.edu/chungsangng>

tral role in the fundamental process of magnetic reconnection, which has been extensively studied in the space physics, plasma physics, and astrophysics communities for decades.^{48–61} One consequence of kinetic physics during reconnection is the formation of small kinetic scale structures, as seen by many kinetic simulations of reconnection.^{62–71} While most kinetic simulations are still in 2D due to high computing costs, larger 3D kinetic simulations using PIC method have been performed in recent years and have found that some of these structures having the geometric form of magnetic flux ropes in 3D.⁷² Physically, such flux ropes are simply 3D counterparts of plasmoids (or secondary islands) seen in 2D reconnection simulations, either kinetic,⁶³ or even in resistive magnetohydrodynamics (MHD).^{73,74}

Besides observations of possible BGK modes mentioned above, there have been more observations of small-scale kinetic structures in the magnetosphere in the last few years,^{75–83} from spacecraft such as the Magnetospheric Multiscale (MMS) Mission.

Motivated by the formation of kinetic flux ropes seen in 3D simulations, we have generalized the form of exact 2D BGK mode solutions further, now with the distribution function also depending on the z -component (along the symmetric axis) of the canonical momentum. Such more general solutions thus allow a parallel current density with associated azimuthal magnetic field. The resulting structures are then of the form of magnetic flux ropes, due to kinetic physics, rather than MHD. We present the analytic forms of such solution in Section II. Some solutions will then be solved numerically in Section III to show properties of solutions as examples. Discussions and conclusion will be presented in Section IV.

II. CONSTRUCTION OF SOLUTIONS

We start the construction of BGK mode solutions by requiring the s -charge species to satisfy the Vlasov Equation

$$\frac{\partial f_s}{\partial t} + \mathbf{v} \cdot \frac{\partial f_s}{\partial \mathbf{r}} + \frac{q_s}{m_s} (\mathbf{E} + \mathbf{v} \times \mathbf{B}) \cdot \frac{\partial f_s}{\partial \mathbf{v}} = 0, \quad (1)$$

where $s = e$ for electrons, and $s = i$ for ions. Note that $q_e = -e$ is a negative value for the electron charge, and m_e is the mass of electron. In this paper, we continue to follow the usual simplification of setting ions to be forming a uniform background of positive ion charge density $n_0 e$ to maintain charge neutrality outside the localized BGK mode structure.²¹ One situation this approximation is justified is when the electrons, imbedded with the BGK structure, are drifting through a uniform background of ions with high enough relative velocity such that ions cannot respond significantly due to the heavier ion mass during the short transit time. This approximation is also valid in the limit of large ion to electron temperature ratio, even without a large relative drift between

ions and electrons. While this assumption seems drastic, it has been found that qualitatively similar solutions still exist for a large range of ion to electron temperature ratio,⁸⁴ which will be the subject of a future publication. By using the form of the Vlasov Equation in Eq. (1), we have assumed a non-relativistic treatment. This is because the numerical construction of BGK mode solutions for the relativistic Vlasov Equation is much more complicated. For BGK modes, we seek steady-state solutions and thus we ignore the time derivative term. We also seek self-consistent solutions so that the electric field \mathbf{E} and the magnetic field \mathbf{B} in Eq. (1) are solved from the Gauss Law $\nabla \cdot \mathbf{E} = \rho_q / \epsilon_0$ and the steady-state Ampère Law $\nabla \times \mathbf{B} = \mu_0 \mathbf{J}$, with charge density ρ_q and current density \mathbf{J} calculated from integrating the moments of the distribution function f_e . Introducing electric potential ψ and magnetic potential \mathbf{A} such that $\mathbf{E} = -\nabla \psi$ and $\mathbf{B} = \nabla \times \mathbf{A}$, the Gauss Law (Poisson equation) and the Ampère Law become

$$\nabla^2 \psi = -\frac{e}{\epsilon_0} \left[n_0 - \int d\mathbf{v} f_e \right], \quad (2)$$

$$\nabla \times \nabla \times \mathbf{A} = -e\mu_0 \int d\mathbf{v} f_e \mathbf{v}, \quad (3)$$

where we have ignored possible current density due to the background ions, assuming the drift velocity between electrons and ions is much smaller than the electron thermal velocity.

Since we are looking for 2D cylindrically symmetric solutions, it is convenient to use cylindrical coordinates, with the z -axis being the symmetric axis. Therefore, only the radial coordinate ρ enters into the spatial dependence of all physical quantities. The steady-state Vlasov Equation can then be written explicitly as

$$v_\rho \frac{\partial f_e}{\partial \rho} + \left\{ \frac{e}{m_e} \left[\frac{d\psi}{d\rho} - \frac{v_\phi}{\rho} \frac{d(\rho A_\phi)}{d\rho} - v_z \frac{dA_z}{d\rho} \right] + \frac{v_\phi^2}{\rho} \right\} \frac{\partial f_e}{\partial v_\rho} - \left[\frac{v_\rho v_\phi}{\rho} - \frac{ev_\rho}{m_e} \frac{d(\rho A_\phi)}{\rho d\rho} \right] \frac{\partial f_e}{\partial v_\phi} + \frac{ev_\rho}{m_e} \frac{dA_z}{d\rho} \frac{\partial f_e}{\partial v_z} = 0, \quad (4)$$

with $\mathbf{A} = A_\phi \hat{\phi} + A_z \hat{z}$ and $\mathbf{v} = v_\rho \hat{\rho} + v_\phi \hat{\phi} + v_z \hat{z}$. Before we continue the construction of solutions for this equation, we introduce the following units to normalize physical quantities to shorten expressions in analysis, as well as in numerical codes. We will measure velocity \mathbf{v} in the unit of electron thermal velocity v_e of the background (far away from the electrostatic structure) Maxwellian electrons, spatial vector \mathbf{r} in the unit of the Debye length $\lambda = v_e / \omega_{pe} = (v_e / e) \sqrt{\epsilon_0 m_e / n_0}$ (with ω_{pe} being the electron plasma frequency), electric potential ψ in the unit of $n_0 e \lambda^2 / \epsilon_0$, electron distribution function f_e in the unit of n_0 / v_e^3 , and magnetic field \mathbf{B} in the unit of $n_0 e \lambda / \epsilon_0 v_e$, with units of other quantities derived from combinations of these units. Note that a magnetic field with a field strength of unity ($B = 1$) in this unit indicates a case where the electron cyclotron frequency equal to ω_{pe} . The Vlasov equation in these units is simply given by Eq. (4) without the need of writing out the e/m_e factors.

For the 2D case with cylindrical symmetry, the steady-state Vlasov equation can be solved by a f_e that depends only on conserved quantities. Therefore, we seek solutions of the general form of $f_e = f(w, l, p)$, where $w = v^2/2 - \psi = (v_\rho^2 + v_\phi^2 + v_z^2)/2 - \psi$ is the normalized total (kinetic plus electrostatic) energy of a particle, $l = 2\rho(v_\phi - A_\phi)$ is two times the z -component of the normalized canonical angular momentum, and $p = v_z - A_z$ is the z -component of the normalized canonical momentum. Note that solutions in Ref. 25 is for the special case without the p dependence. This generalization turns out to be non-trivial since the p dependence will generally induce a current along the z -axis which in turn produces an azimuthal magnetic field and thus the flux rope structure. So this should be the more general case in physical situations. To complete the solution, f_e of this form must also satisfies self-consistently the Gauss Law (2) and the Ampère Law (3), which can be written explicitly as

$$\frac{1}{\rho} \frac{d}{d\rho} \left(\rho \frac{d\psi}{d\rho} \right) = \int d^3v f(w, l, p) - 1, \quad (5)$$

$$\frac{d}{d\rho} \left[\frac{1}{\rho} \frac{d}{d\rho} (\rho A_\phi) \right] = \beta_e^2 \int d^3v f(w, l, p) v_\phi, \quad (6)$$

$$\frac{1}{\rho} \frac{d}{d\rho} \left(\rho \frac{dA_z}{d\rho} \right) = \beta_e^2 \int d^3v f(w, l, p) v_z, \quad (7)$$

where $\beta_e^2 = v_e^2/c^2$ is the square of the ratio of the electron thermal velocity to the speed of light. These three equations are much more complicated than simply three coupled ordinary differential equations, as their forms seem to suggest. This is due to the fact that f is an unknown function that depends on ψ , A_ϕ , and A_z . Therefore this is a set of three coupled nonlinear integral-differential equations, with the possibility of having many non-trivial solutions. The fact that we are using a non-relativistic treatment might suggest simply setting $\beta_e^2 = 0$, so that Eqs. (6) and (7) imply special solutions of $A_\phi = B_{z0}\rho/2$, $A_z = \text{constant}$, or simply a uniform magnetic field along the z -direction with a field strength of B_{z0} . This limit is essentially considering the electrostatic effect only, which is indeed the dominant effect. However, for solutions having flux rope structures, we require the self-generated non-uniform magnetic field. Therefore we will consider a large enough β_e^2 but still within the validity of the non-relativistic treatment.

Due to the (maybe infinitely) large number of acceptable forms of the function f , we will first show the existence of solutions by limiting it to a form of

$$f(w, l, p) = (2\pi)^{-3/2} e^{-w} \left(1 - h e^{-kl^2 - \xi p^2} \right), \quad (8)$$

where $-\infty < h < 0$ or $0 < h < 1$, $k > 0$, $\xi > 0$ are constant parameters. The case of $h = 0$ is excluded explicitly due to the non-existence of localized solutions as proved in Ref. 24. This form with the specified ranges of parameters is chosen to ensure $\infty > f \geq 0$ for any ρ and \mathbf{v} values, since physically it is a distribution function, and that f tends to a Maxwellian (with the already specified

thermal velocity) as $\rho \rightarrow \infty$ (assuming $\psi \rightarrow 0$, and the magnetic field tends to a uniform field, in the same limit) so that the solution represents a localized structure in the transverse directions. Moreover, this form of f would allow the integration of its moments easier, and resulting in analytic expressions in the right-hand-sides of Eqs. (5) to (7). While this is one of many possible forms, it already have three parameters that allows solutions to have a large range of properties that require an extensive scan of the parameter space to fully explore. Obvious generalizations of this form include adding terms with different h , k , and ξ , or adding terms with more general dependence in l or p in the exponential function. However, due to the nonlinear nature of this set of equations, it is unlikely to expand f with a complete set of functions. We will therefore only consider the form given by Eq. (8) in the rest of this paper.

Once we have specified the form of f using Eq. (8), we can then evaluate its moments to be used in Eqs. (5) to (7). The zeroth order moment gives the normalized electron density $n_e = \int d^3v f(w, l, p)$, with an analytic expression after integration

$$n_e = e^\psi \left[1 - \frac{h \exp \left(-\frac{4kA_\phi^2 \rho^2}{1+8k\rho^2} - \frac{\xi A_z^2}{1+2\xi} \right)}{\sqrt{(1+8k\rho^2)(1+2\xi)}} \right], \quad (9)$$

which can be substituted as the first term on the right-hand-side of Eq. (5). Note that n_e is always positive with the restrictions on parameters mentioned above. Also, $n_e \rightarrow 1$ as $\rho \rightarrow \infty$, indicating a localized structure as required. The expression in Eq. (9) gives further restrictions for the existence of a localized ψ ,

$$1 \geq e^{\psi(0)} \left[1 - \frac{h}{\sqrt{1+2\xi}} \exp \left(-\frac{\xi A_z^2(0)}{1+2\xi} \right) \right], \quad (10)$$

with $\psi(0)$ and $A_z(0)$ being ψ and A_z at $\rho = 0$, for positive/negative h and $\psi(0)$.

Similarly, the first order moments give the normalized current density $\mathbf{J} = J_\phi \hat{\phi} + J_z \hat{z}$, where $J_\phi = -\int d^3v f(w, l, p) v_\phi$, and $J_z = -\int d^3v f(w, l, p) v_z$. The normalized electron flow velocity is then given by $\bar{\mathbf{v}} = -\mathbf{J}/n_e$. In the same way, J_ϕ and J_z can be integrated into analytic forms

$$J_\phi = \frac{8hkA_\phi \rho^2 e^\psi}{(1+8k\rho^2)^{3/2} \sqrt{1+2\xi}} \exp \left(-\frac{4kA_\phi^2 \rho^2}{1+8k\rho^2} - \frac{\xi A_z^2}{1+2\xi} \right),$$

$$J_z = \frac{2h\xi A_z e^\psi}{\sqrt{1+8k\rho^2} (1+2\xi)^{3/2}} \exp \left(-\frac{4kA_\phi^2 \rho^2}{1+8k\rho^2} - \frac{\xi A_z^2}{1+2\xi} \right),$$

which can then be substituted into Eqs. (6) and (7) respectively. With these analytic integrations, the right-hand-sides of Eqs. (5) to (7) become explicit functions of ψ , A_ϕ , and A_z such that they are a set of three coupled nonlinear ordinary differential equations that can be integrated numerically with a technique described in Refs. 24 and 25.

The second or higher order moments are not required in solving for solutions. However, for completeness and possible comparison with either observation data or direct simulations, we will calculate the second order moments in terms of the normalized electron pressure tensor $\mathbf{P} = \int d^3v f(w, l, p) (\mathbf{v} - \bar{\mathbf{v}})(\mathbf{v} - \bar{\mathbf{v}})$, which is in the unit of $n_0 k_B T_{e0}$ with $T_{e0} \equiv m_e v_e^2 / k_B$ and k_B being the Boltzmann constant. Expressing \mathbf{P} in cylindrical coordinates, it is easy to show that $P_{\rho\phi} = P_{\phi\rho} = P_{\rho z} = P_{z\rho} = 0$, and $P_{\rho\rho} = n_e$. Other components are given by

$$\begin{aligned} P_{\phi\phi} + n_e \bar{v}_\phi^2 &= e^\psi \left\{ 1 - h \left[\frac{1 + 8k\rho^2 + (8kA_\phi\rho^2)^2}{(1 + 8k\rho^2)^{5/2} \sqrt{1 + 2\xi}} \right] \right. \\ &\quad \left. \exp \left(-\frac{4kA_\phi^2\rho^2}{1 + 8k\rho^2} - \frac{\xi A_z^2}{1 + 2\xi} \right) \right\}, \\ P_{zz} + n_e \bar{v}_z^2 &= e^\psi \left\{ 1 - h \left[\frac{1 + 2\xi + (2\xi A_z)^2}{(1 + 2\xi)^{5/2} \sqrt{1 + 8k\rho^2}} \right] \right. \\ &\quad \left. \exp \left(-\frac{4kA_\phi^2\rho^2}{1 + 8k\rho^2} - \frac{\xi A_z^2}{1 + 2\xi} \right) \right\}, \\ P_{\phi z} + n_e \bar{v}_\phi \bar{v}_z &= -\frac{16hk\xi A_\phi A_z \rho^2}{(1 + 2\xi)^{3/2} (1 + 8k\rho^2)^{3/2}} \\ &\quad \exp \left(\psi - \frac{4kA_\phi^2\rho^2}{1 + 8k\rho^2} - \frac{\xi A_z^2}{1 + 2\xi} \right), \quad (11) \end{aligned}$$

with $P_{z\phi} = P_{\phi z}$. Clearly as $\rho \rightarrow \infty$, $P_{\rho\rho} = P_{\phi\phi} = P_{zz} \rightarrow 1$, with other components being zero. We can also define normalized parallel and perpendicular electron temperature, in the unit of $k_B T_{e0}$, with $T_{e\parallel} \equiv P_{zz}/n_e$, and $T_{e\perp} \equiv (P_{\rho\rho} + P_{\phi\phi})/2n_e$. The total normalized electron temperature is then $T_e \equiv (T_{e\parallel} + 2T_{e\perp})/3$.

III. NUMERICAL EXAMPLES

In this section, we will present some numerical examples to show that solutions constructed by the method described in Section II do exist. We have mentioned already that this group of solutions depend on a number of parameters: h , k , ξ , and β_e . Moreover, in addition to the boundary condition of $\psi \rightarrow 0$ as $\rho \rightarrow \infty$ required for a localized solution, two more free parameters are needed for boundary conditions. In our method of integration, we specify $A_z(0)$ and $B_z(0) = 2dA_\phi(0)/d\rho$ on the symmetric axis as those boundary values. Note that $A_\phi(0)$, $d\psi(0)/d\rho$, and $dA_z(0)/d\rho$ are zero by symmetry. The value $\psi(0)$ is determined numerically to satisfy the condition for a localized solution as described in Refs. 24 and 25. Because of a large parameter space with these six parameters, it is difficult to investigate how properties of solutions depend on these parameters, although we have simulated a large number of cases with different parameters to confirm that solutions do exist generally. In this section however, we will present only two examples for brevity, to demonstrate explicitly the existence of

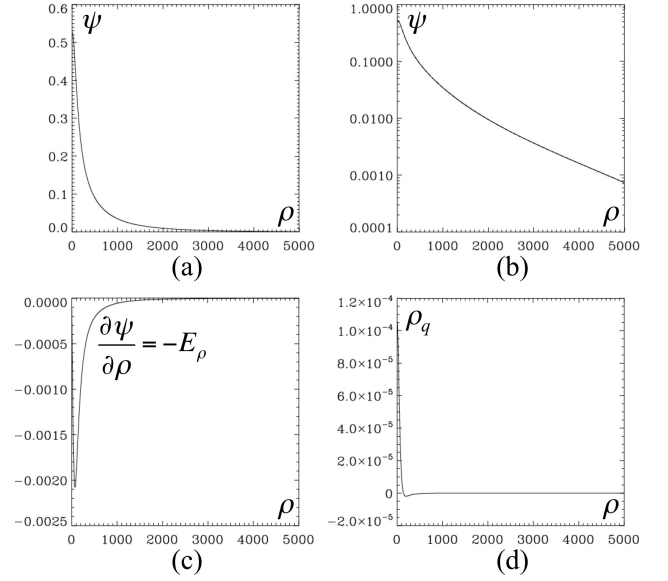


FIG. 1. (a) ψ , (b) ψ in semi-log scales, (c) $d\psi/d\rho$, (d) ρ_q as functions of ρ , for a case with $h = 0.99$, $k = 1 \times 10^{-5}$, $\xi = 1$, $\beta_e = 0.005$, $A_z(0) = 1$, and $B_z(0) = 0.00293$.

solutions, and to point out some of their properties. The first example is for a positive electric potential ψ with $h > 0$, while the other one is for a negative ψ with $h < 0$.

Fig. 1 shows plots of ψ , $d\psi/d\rho$, which is the negative of the normalized radial electric field E_ρ , and the normalized charge density ρ_q as functions of the radial coordinate ρ , for the first case with $h = 0.99$, $k = 1 \times 10^{-5}$, $\xi = 1$, $\beta_e = 0.005$, $A_z(0) = 1$, and $B_z(0) = 0.00293$. We have plotted over a range of ρ from 0 to 5000, in the unit of λ_D , to show clearly the structures of the solution well into the asymptotic regime where $\psi \rightarrow 0$. The length scale l_ψ over which $\psi > 0.1\psi(0)$ is about $\rho < l_\psi \sim 700$, while the length scale l_q over which $\rho_q > 0.1\rho_q(0)$ is about $\rho < l_q \sim 100$. This example shows that the electrostatic structure and the region of charge non-neutrality can be much greater than λ_D , although there are also many other choices of parameters in which length scales are of the order of λ_D . Another spatial unit that can be used to measure such kinetic structures is the electron inertia length $d_e = c/\omega_{pe} = \lambda_D/\beta_e$. For this case, we have $d_e = 200\lambda_D$ so that the range of ρ is 0 to $25d_e$ in Fig. 1, and $l_\psi \sim 3.5d_e$, $l_q \sim 0.5d_e$. Note that $l_q \ll l_\psi$ is expected since the electric potential is due to the charge non-neutrality through the Poisson equation. Fig. 1 (b) shows the plot of ψ again in semi-log scales to show better the asymptotic behavior of ψ as $\rho \rightarrow \infty$. In fact, from Eq. (5) with Eq. (9), it can be shown that $\psi \propto \exp(-\rho)/\sqrt{\rho}$ in this limit. From Fig. 1 (d) we see that ρ_q becomes negative outside the positive core with a radius about l_q . In fact the whole structure must be charge neutral, as required by the asymptotic behavior of the electric field which tends to zero exponentially at large ρ . Fig. 1 (c) shows that the positive radial electric

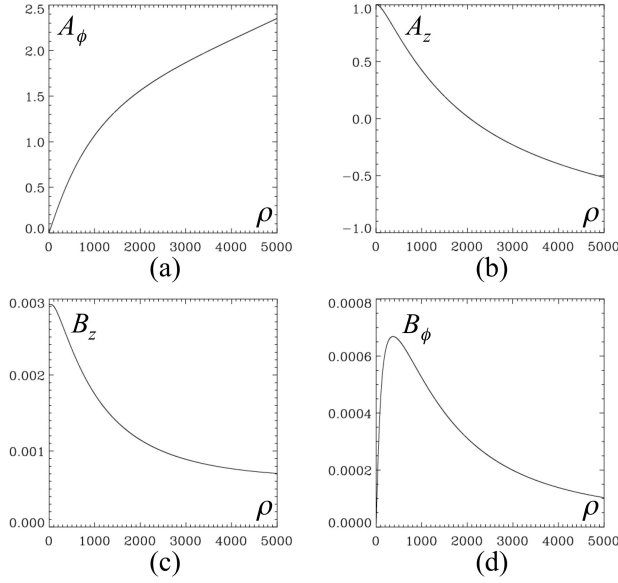


FIG. 2. (a) A_ϕ , (b) A_z , (c) B_z , (d) B_ϕ as functions of ρ , for the same case as Fig. 1.

field E_ρ peaks around the edge of the core with positive charge density around $\rho \sim l_q$, and tends to zero over a wider tail of the order of l_ψ . For this case, the values of ρ_q is very small, with a maximum about 10^{-4} . However, such a small ρ_q can still produce a significant ψ since it is non zero over a larger range of ρ . With such a small ρ_q , the normalized electron density $n_e = 1 - \rho_q$ is very close to unity. Therefore we do not show a plot of n_e here.

Fig. 2 shows plots of magnetic potential components A_ϕ , A_z and corresponding magnetic field components $B_z = [d(\rho A_\phi)/d\rho]/\rho$, $B_\phi = -dA_z/d\rho$ for the same case. Asymptotically as $\rho \rightarrow \infty$, $A_\phi \rightarrow B_\infty \rho/2$ and $A_z \rightarrow -C_1 \ln \rho + C_2$ with B_∞ , C_1 and C_2 being constants, so that $B_z \rightarrow B_\infty$, and $B_\phi \rightarrow C_1/\rho$, i.e., a uniform field along the z -direction. We can see that the length scale of the magnetic field structure is much larger than the length scale of the electric structure l_ψ and charge non-neutrality structure l_q . This is expected since a plasma has a tendency to neutralize charge separation and to shield electric field, but does not neutralize current density and does not shield magnetic field produced by net currents.

Fig. 3 (a) and (b) shows plots of the normalized current density components J_ϕ and J_z , corresponding to the magnetic field shown in Fig. 2 (c) and (d), through the Ampère Law (6) and (7). As pointed out above, n_e is very close to unity for this case, so the normalized current density \mathbf{J} is essentially the negative of the normalized electron flow velocity $\bar{\mathbf{v}}$. It is also easy to check that the sign of \mathbf{J} is consistent with the \mathbf{B} profile. Since J_ϕ is positive and localized, it produces an increase of B_z on the z -axis. Asymptotically B_z tends to a constant value B_∞ , presumably given by the background magnetic field. At the same time, a positive localized J_z produces a positive

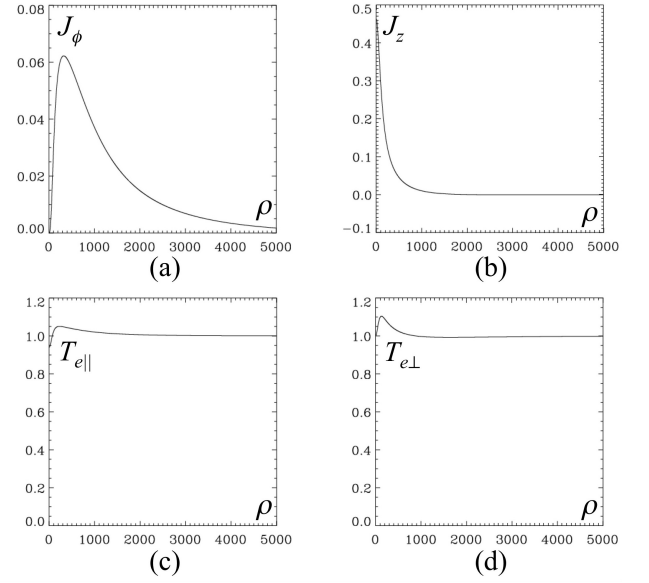


FIG. 3. (a) J_ϕ , (b) J_z , (c) $T_{e||}$, (d) $T_{e\perp}$ as functions of ρ , for the same case as Fig. 1.

localized B_ϕ which tends to an asymptotic $1/\rho$ behavior at large ρ , as consistent with a localized axial current. For completeness, the normalized parallel and perpendicular electron temperatures $T_{e||}$ and $T_{e\perp}$ are plotted in Fig. 3 (c) and (d). They are given by the calculations of the components of the normalized electron pressure tensor through Eqs. (11). We see that they deviate from unity (background) over a region of a length scale close to l_ψ . While the deviation is not large for this case, of the order of 10%, it is large enough to be observable if such solutions exist in real physical situations.

With ψ , A_ϕ , and A_z solved from Eqs. (5), (6), and (7), the corresponding normalized electron distribution f_e can be calculated through Eq. (8). For this symmetric solution, the phase space of f_e is four-dimensional in v_ρ , v_ϕ , v_z , and ρ . However, since the dependence on v_ρ is simply a gaussian factor $\exp(-v_\rho^2/2)$, non-trivial behavior is in the v_ϕ , v_z , and ρ space only. Due to the difficulty in plotting f_e in the full three-dimensional space, we will instead plot a few 2D cross sections to illustrate some features of the full structure. Fig. 4 (a) shows a color coded contour plot for the cross section of $\ln f_e$ on the plane of v_z vs. v_ϕ at $\rho = v_\rho = 0$, while Fig. 4 (b) shows a similar plot but at $\rho = 400$, where ψ has not decreased to a small level with B_ϕ and J_ϕ near maximum. In these contour plots, we employed a rainbow color coding scheme with the dark violet end of the spectrum at the minimum value (l_{\min}) of $\ln f_e$ over the plot area, and the red end of the spectrum at the maximum value (l_{\max}) of $\ln f_e$ over the plot area, increasing over 30 contour levels with an increment of Δl at each level. For Fig. 4 (a), $l_{\min} = -9.34$, $l_{\max} = -2.46$, and $\Delta l = 0.229$, while $l_{\min} = -7.7$, $l_{\max} = -2.68$, and $\Delta l = 0.167$ for Fig. 4 (b). We report these numbers here instead of showing a color bar for each plot because such

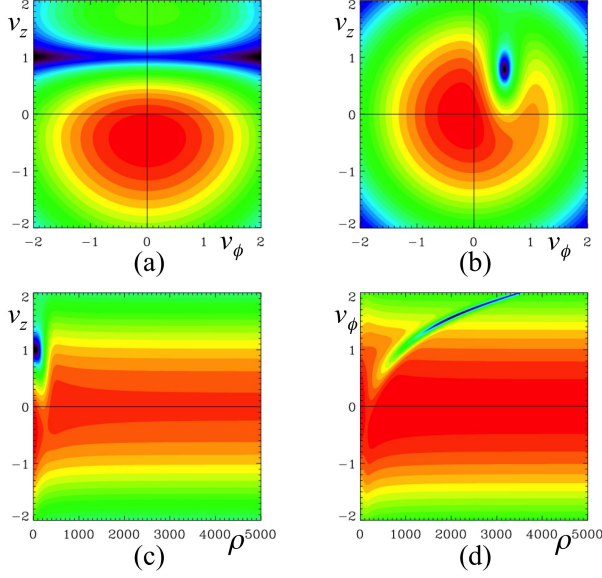


FIG. 4. Color coded contour plots for the cross section of $\ln f_e$ on the planes of (a) v_z vs. v_ϕ at $\rho = v_\rho = 0$, (b) v_z vs. v_ϕ at $\rho = 400$, $v_\rho = 0$, (c) v_z vs. ρ at $v_\phi = v_\rho = 0$, (d) v_ϕ vs. ρ at $v_z = v_\rho = 0$, for the same case as Fig. 1.

bars would be difficult to read or taking up too much space, while these numbers would allow the determination of the value of $\ln f_e$ at any point if needed.

From these two plots, we see from the shift of the contours with larger values that there is an electron flow with a negative z -component both on the axis ($\rho = 0$), and slightly off axis, and a negative ϕ -component off axis but zero on the axis as required by symmetry. These features are consistent with the plots of J_ϕ and J_z in Fig. 3. We also see in Fig. 4 (b) an interesting feature of a hole-like structure of electron depletion in the v_ϕ - v_z space, indicating a strong distortion from an isotropic distribution as in a Maxwellian. Fig. 4 (c) shows the cross section on the plane of v_z vs. ρ at $v_\phi = v_\rho = 0$, with $l_{\min} = -8.61$, $l_{\max} = -2.67$, and $\Delta l = 0.198$, while Fig. 4 (d) shows the cross section on the plane of v_ϕ vs. ρ at $v_z = v_\rho = 0$, with $l_{\min} = -7.35$, $l_{\max} = -2.46$, and $\Delta l = 0.163$. Electron depletions are seen in these two plots also, with a structure more localized in ρ shown in Fig. 4 (c), while the structure extends to much large ρ values. This is consistent with a narrower profile in J_z but a more extended profile in J_ϕ shown in Fig. 3.

With the components of magnetic field B_z and B_ϕ shown in Fig. 2 (c) and (d), it is clear that the magnetic field lines are having a helical structure as in a flux rope. To illustrate this explicitly, Fig. 5 shows some magnetic field lines drawn in different colors, going through $y = z = 0$, $x = 0, 2.5, 5, 10, 20 d_e$ over a range of positive z values. We use d_e as the spatial unit for this plot, instead of λ_D as in previous plots, for clarity in the labels, and to show that the helical flux rope structure has a spatial scale of a few d_e . Since $B_\phi = 0$ at $\rho = 0$ by symmetry,

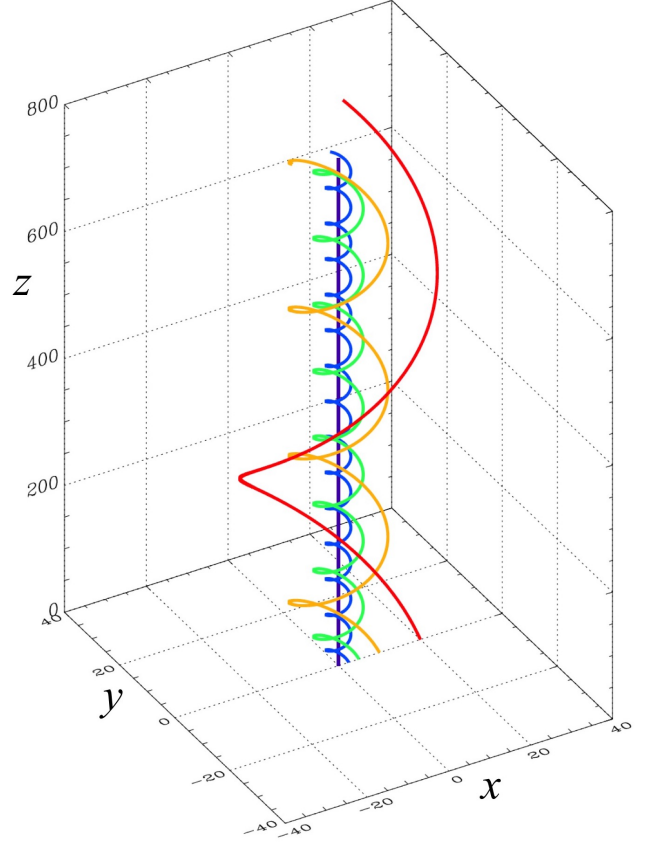


FIG. 5. Five magnetic field lines drawn in different colors, going through $y = z = 0$, $x = 0, 2.5, 5, 10, 20 d_e$, which is $200 \lambda_D$, the unit of ρ in previous plots, for the same case as Fig. 1.

the magnetic field on the z -axis is going straight along the axis. Similarly, since $B_z \rightarrow B_\infty$ while $B_\phi \rightarrow C_1/\rho$ as $\rho \rightarrow \infty$, the magnetic field lines also tend to uniform field along the z -direction asymptotically. Therefore the helical flux rope structure with larger B_ϕ is localized to a range of ρ approximately between $1 d_e$ and $10 d_e$.

For the second case, Figs. 6 to 9 show plots corresponding to Figs. 1 to 4 for a case with $h = -1$, $k = 1 \times 10^{-5}$, $\xi = 1$, $\beta_e = 0.005$, $A_z(0) = 1$, and $B_z(0) = 0.00293$. We see from these plots that many features for this case are very similar to the first case except with opposite sign. The spatial scales of structures are actually similar but we plot in Figs. 6 to 9 using a range of ρ from 0 to $2000 \lambda_D$ instead of $5000 \lambda_D$ as in Figs. 1 to 4 to show more clearly features near the axis for comparison. Electric potential ψ and electric field E_ρ , as well as charge density ρ_q , shown in Fig. 6 are with signs negative to corresponding quantities shown in Fig. 1, although not with exactly the same magnitudes. B_z shown in Fig. 7 (c) still has positive sign by choice but is having a dip in value on and near the $\rho = 0$ axis, opposite to an increase shown in Fig. 2 (c). B_ϕ for this case shown in Fig. 7 (d) is now pointing to the negative direction, opposite to the first

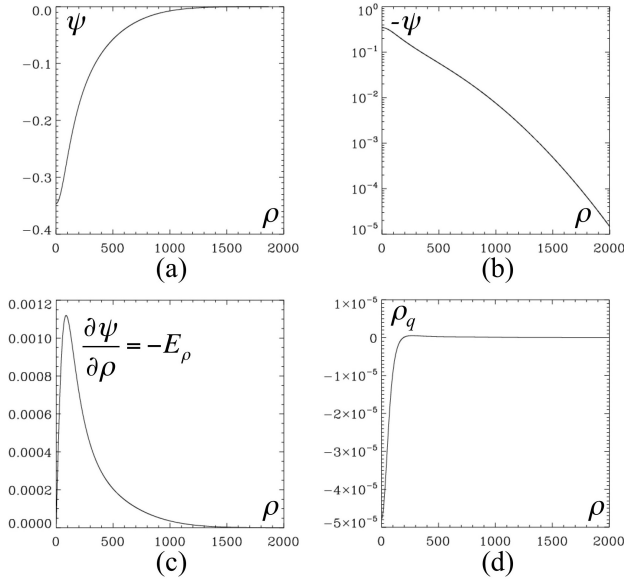


FIG. 6. (a) ψ , (b) $-\psi$ in semi-log scales, (c) $d\psi/d\rho$, (d) ρ_q as functions of ρ , for a case with $h = -1$, $k = 1 \times 10^{-5}$, $\xi = 1$, $\beta_e = 0.005$, $A_z(0) = 1$, and $B_z(0) = 0.00293$.

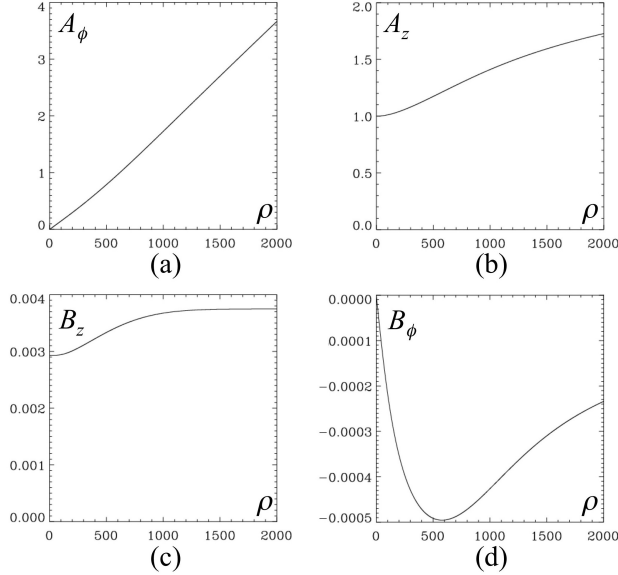


FIG. 7. (a) A_ϕ , (b) A_z , (c) B_z , (d) B_ϕ as functions of ρ , for the same case as Fig. 6.

case shown in in Fig. 2 (d).

These opposite features in the magnetic field is indeed due to current density components J_ϕ and J_z having negative sign, as shown in Fig. 8 (a) and (b), opposite to corresponding plots shown in Fig. 3 (a) and (b) for the first case. The normalized parallel and perpendicular electron temperatures $T_{e\parallel}$ and $T_{e\perp}$ plotted in Fig. 8 (c) and (d) are also having different profiles than those in Fig. 3 (c) and (d), although not exactly opposite.

Cross section plots of $\ln f_e$ for this case shown in Fig. 9

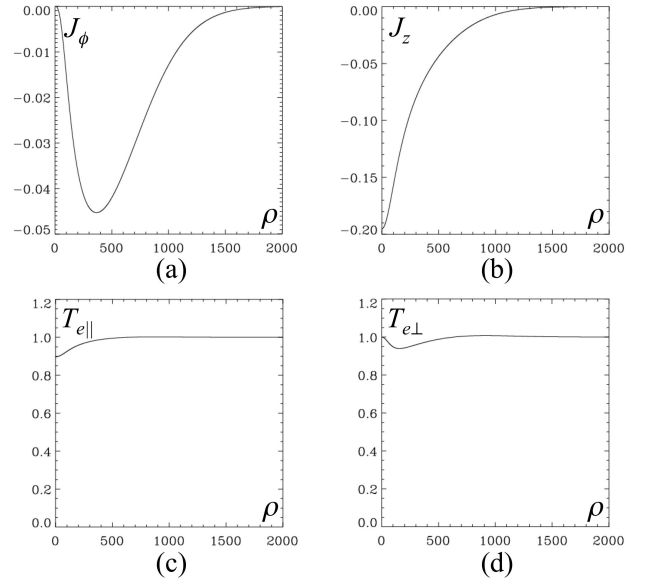


FIG. 8. (a) J_ϕ , (b) J_z , (c) $T_{e\parallel}$, (d) $T_{e\perp}$ as functions of ρ , for the same case as Fig. 6.

are also very different from corresponding plots shown in Fig. 4. We first list color code values to read these plots: $l_{\min} = -7.1$, $l_{\max} = -2.64$, and $\Delta l = 0.148$ for Fig. 9 (a); $l_{\min} = -6.84$, $l_{\max} = -2.61$, and $\Delta l = 0.141$ for Fig. 9 (b); $l_{\min} = -4.98$, $l_{\max} = -2.65$, and $\Delta l = 0.0777$ for Fig. 9 (c); $l_{\min} = -6.84$, $l_{\max} = -2.55$, and $\Delta l = 0.143$ for Fig. 9 (d). This case with $h = -1$ means that now electrons are added to the Boltzmann distribution, rather than taking away in the first case with $h = 0.99$, as can be seen from the form of the distribution specified in Eq. (8). Therefore we see from Fig. 9 increases of electrons in regions corresponding to electron depletions shown in Fig. 4. Similar to the discussion on Fig. 4, the shift of the electron distribution seen in Fig. 9 is consistent with the sign of the current density plotted in Fig. 8.

IV. DISCUSSION AND CONCLUSION

In this paper, we have presented a general theory in constructing localized 2D BGK modes, which are exact solutions of the Vlasov-Poisson-Ampère system of equations, with electron distribution functions depending on three conserved quantities: energy, canonical angular momentum, and canonical momentum along the symmetric axis. These 2D solutions generally have a magnetic field in both the axial and azimuthal directions and thus a structure in the form of a flux rope in the kinetic scales. We emphasize that such flux rope solutions are solved from the kinetic theory (Vlasov equation) and thus are very different from flux rope solutions in MHD.

To show the existence of solutions based on this theory, and to illustrate some general features in solutions, we

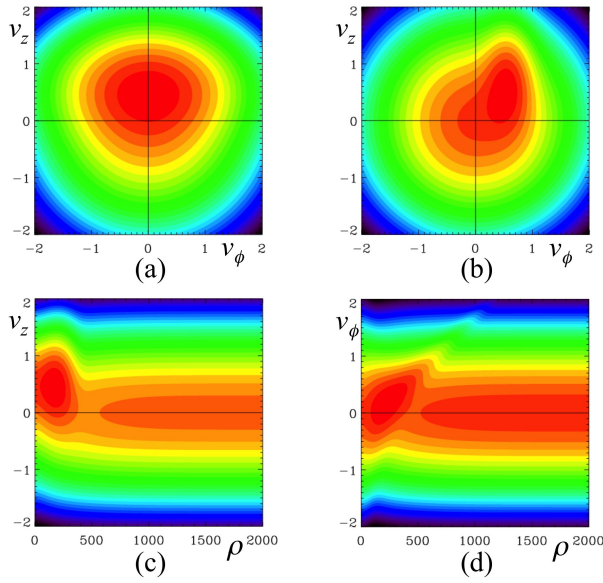


FIG. 9. Color coded contour plots for the cross section of $\ln f_e$ on the planes of (a) v_z vs. v_ϕ at $\rho = v_\rho = 0$, (b) v_z vs. v_ϕ at $\rho = 400$, $v_\rho = 0$, (c) v_z vs. ρ at $v_\phi = v_\rho = 0$, (d) v_ϕ vs. ρ at $v_z = v_\rho = 0$, for the same case as Fig. 6.

have presented two solutions found numerically based on a special form of solution specified in Eq. (8). This form of solutions depends on six parameters. The two examples are chosen with only one parameter being different: $h = 0.99$ for the first case, which can be described physically as taking away electrons so that electron holes form in the electron distribution, while $h = -1$ for the second case, which has electrons added instead. While magnetic flux rope structures exist in both cases, electric potential and electric fields, as well as current density and magnetic field perturbations are having opposite signs, most noticeably an increase of magnetic field on the axis for the first case, but a decrease for the second case. Correspondingly there is a decrease of the electron density n_e on the axis for the first case, but an increase for the second case, although $n_e \approx 1$ with our choices of parameters in our examples.

The second case with a negative potential ψ deserves some more discussion. Such localized electrostatic structure of negative electric potential produced by electron dynamics with a uniform ion background does not exist in the conventional 1D BGK mode solution, since the existent of a self-consistent solution in that case depends on having trapping electrons with a different form of distribution from the Boltzmann distribution of passing electrons. However, a localized negative electric potential cannot trap electrons and thus all electrons are having the same Boltzmann distribution which cannot support a self-consistent negative potential structure. The fact that a solution with a negative potential exists as a 2D BGK mode is interesting in itself. Moreover, there is an indication that a negative potential solution might be

easier to exist than a positive one in the sense that the range of h for the positive case in our form of solutions is $0 < h < 1$, while it is $-\infty < h < 0$ for the negative potential case. Physically it means that while there is a limit in taking electrons away from a Boltzmann distribution since the most one can do is to decrease it to zero, there is no limit in adding electrons in the negative potential case.

We again emphasize that the two examples presented in this paper are simply two choices of parameters out of a large six-dimensional parameter space, and thus there can be solutions with very different properties from these two examples. Moreover, as have been pointed out above, our form of the electron distribution in Eq. (8) can be easily generalized to forms with many more parameters. Due to the non-linear nature of such solutions, such generalizations most likely will produce different solutions. Adding to the complication is the ion dynamics, which is ignored in this paper with the assumption of a uniform ion background. There is one more possible generalization in extending the form of the electron distribution from a smooth and analytic ones such as in Eq. (8) to possible discontinuous ones such as in 1D BGK mode theory after taking into account of the possibility of trapping electrons having a different distribution. The physics of trapping (in transverse directions only) is ignored in this paper but it can indeed be included in a more general case.

With the possibility of the existent of 2D BGK mode solutions over a very large parameter space, it is interesting to see whether such solutions can be compared with observations in space or experiments. However, this also depends on the stability of such solutions, as well as the existent of mechanisms that can generate such solutions. In this paper, we have only considered the existent of steady-state solutions, without considering whether such solutions are stable and how such solutions can be formed. While these are interesting and important topics for further research, our solutions can also be used to compare with large-scale numerical simulations using either the Vlasov equation or PIC method, in which flux ropes in kinetic scales have been observed.

ACKNOWLEDGMENTS

This work is partially supported by a National Science Foundation grant PHY-1004357.

¹T. M. O'Neil and F. V. Coroniti, "The collisionless nature of high-temperature plasmas," *Rev. Mod. Phys.* **71**, S404–S410 (1999), <https://doi.org/10.1103/RevModPhys.71.S404>.

²V. M. Vasyliunas, "A survey of low-energy electrons in the evening sector of the magnetosphere with ogo 1 and ogo 3," *Journal of Geophysical Research* (1896-1977) **73**, 2839–2884 (1968), <https://agupubs.onlinelibrary.wiley.com/doi/pdf/10.1029/JA073i009p02839>.

³M. P. Leubner, "Fundamental issues on kappa-distributions in space plasmas and interplanetary proton distributions," *Physics of Plasmas* **11**, 1308–1316 (2004), <https://doi.org/10.1063/1.1667501>.

- ⁴G. Livadiotis and D. J. McComas, "Beyond kappa distributions: Exploiting tsallis statistical mechanics in space plasmas," *Journal of Geophysical Research: Space Physics* **114** (2009), 10.1029/2009JA014352, <https://agupubs.onlinelibrary.wiley.com/doi/pdf/10.1029/2009JA014352>.
- ⁵L. D. Landau, "On the vibrations of the electronic plasma," *J. Phys.(USSR)* **10**, 25–34 (1946), [*Zh. Eksp. Teor. Fiz.*16,574(1946)].
- ⁶C. S. Ng, A. Bhattacharjee, and F. Skiff, "Kinetic eigenmodes and discrete spectrum of plasma oscillations in a weakly collisional plasma," *Phys. Rev. Lett.* **83**, 1974–1977 (1999), <https://doi.org/10.1103/PhysRevLett.83.1974>.
- ⁷C. S. Ng, A. Bhattacharjee, and F. Skiff, "Complete spectrum of kinetic eigenmodes for plasma oscillations in a weakly collisional plasma," *Phys. Rev. Lett.* **92**, 065002 (2004), <https://doi.org/10.1103/PhysRevLett.92.065002>.
- ⁸C. Black, K. Germaschewski, A. Bhattacharjee, and C. S. Ng, "Discrete kinetic eigenmode spectra of electron plasma oscillations in weakly collisional plasma: A numerical study," *Physics of Plasmas* **20**, 012125 (2013), <https://doi.org/10.1063/1.4789882>.
- ⁹I. B. Bernstein, J. M. Greene, and M. D. Kruskal, "Exact nonlinear plasma oscillations," *Phys. Rev.* **108**, 546–550 (1957), <https://doi.org/10.1103/PhysRev.108.546>.
- ¹⁰I. H. Hutchinson, "Electron holes in phase space: What they are and why they matter," *Physics of Plasmas* **24**, 055601 (2017), <https://doi.org/10.1063/1.4976854>.
- ¹¹D. R. Nicholson, *Introduction to plasma theory* (John Wiley & Sons, 1983).
- ¹²D. G. Swanson, *Plasma waves* (CRC Press, 2003).
- ¹³D. A. Gurnett and A. Bhattacharjee, *Introduction to Plasma Physics: With Space, Laboratory and Astrophysical Applications* (Cambridge University Press, 2017).
- ¹⁴R. E. Ergun, C. W. Carlson, J. P. McFadden, F. S. Mozer, L. Muschietti, I. Roth, and R. J. Strangeway, "Debye-scale plasma structures associated with magnetic-field-aligned electric fields," *Phys. Rev. Lett.* **81**, 826–829 (1998), <https://doi.org/10.1103/PhysRevLett.81.826>.
- ¹⁵J. R. Franz, P. M. Kintner, and J. S. Pickett, "Polar observations of coherent electric field structures," *Geophysical Research Letters* **25**, 1277–1280 (1998), <https://agupubs.onlinelibrary.wiley.com/doi/pdf/10.1029/98GL50870>.
- ¹⁶J. R. Franz, P. M. Kintner, J. S. Pickett, and L.-J. Chen, "Properties of small-amplitude electron phase-space holes observed by polar," *Journal of Geophysical Research: Space Physics* **110** (2005), 10.1029/2005JA011095, <https://agupubs.onlinelibrary.wiley.com/doi/pdf/10.1029/2005JA011095>.
- ¹⁷C. A. Cattell, J. Dombeck, J. R. Wygant, M. K. Hudson, F. S. Mozer, M. A. Temerin, W. K. Peterson, C. A. Kletzing, C. T. Russell, and R. F. Pfaff, "Comparisons of polar satellite observations of solitary wave velocities in the plasma sheet boundary and the high altitude cusp to those in the auroral zone," *Geophysical Research Letters* **26**, 425–428 (1999), <https://agupubs.onlinelibrary.wiley.com/doi/pdf/10.1029/1998GL900350>.
- ¹⁸M. Oppenheim, D. L. Newman, and M. V. Goldman, "Evolution of electron phase-space holes in a 2d magnetized plasma," *Phys. Rev. Lett.* **83**, 2344–2347 (1999), <https://doi.org/10.1103/PhysRevLett.83.2344>.
- ¹⁹N. Singh, "Electron holes as a common feature of double-layer-driven plasma waves," *Geophysical Research Letters* **27**, 927–930 (2000), <https://agupubs.onlinelibrary.wiley.com/doi/pdf/10.1029/1999GL003701>.
- ²⁰N. Singh, S. M. Loo, B. E. Wells, and C. Deverapalli, "Three-dimensional structure of electron holes driven by an electron beam," *Geophysical Research Letters* **27**, 2469–2472 (2000), <https://agupubs.onlinelibrary.wiley.com/doi/pdf/10.1029/2000GL003761>.
- ²¹L.-J. Chen, *Bernstein-Greene-Kruskal electron solitary waves in collisionless plasmas*, Ph.D. thesis, UNIVERSITY OF WASHINGTON (2002).
- ²²L.-J. Chen and G. K. Parks, "Bgk electron solitary waves in 3d magnetized plasma," *Geophysical Research Letters* **29**, 45–1–45–4 (2002), <https://agupubs.onlinelibrary.wiley.com/doi/pdf/10.1029/2001GL013385>.
- ²³L.-J. Chen, D. J. Thouless, and J.-M. Tang, "Bernstein-green-kruskal solitary waves in three-dimensional magnetized plasma," *Phys. Rev. E* **69**, 055401 (2004), <https://doi.org/10.1103/PhysRevE.69.055401>.
- ²⁴C. S. Ng and A. Bhattacharjee, "Bernstein-green-kruskal modes in a three-dimensional plasma," *Phys. Rev. Lett.* **95**, 245004 (2005), <https://doi.org/10.1103/PhysRevLett.95.245004>.
- ²⁵C. S. Ng, A. Bhattacharjee, and F. Skiff, "Weakly collisional landau damping and three-dimensional bernstein-green-kruskal modes: New results on old problems," *Physics of Plasmas* **13**, 055903 (2006), <https://doi.org/10.1063/1.2186187>.
- ²⁶Q. M. Lu, B. Lembege, J. B. Tao, and S. Wang, "Perpendicular electric field in two-dimensional electron phase-holes: A parameter study," *Journal of Geophysical Research: Space Physics* **113** (2008), 10.1029/2008JA013693, <https://agupubs.onlinelibrary.wiley.com/doi/pdf/10.1029/2008JA013693>.
- ²⁷C. S. Ng, S. J. Soundararajan, and E. Yasin, "Electrostatic structures in space plasmas: Stability of two-dimensional magnetic bernstein-green-kruskal modes," *AIP Conference Proceedings* **1436**, 55–60 (2012), <https://aip.scitation.org/doi/pdf/10.1063/1.4723590>.
- ²⁸J. P. Lynov, P. Michelsen, H. L. Pécseli, J. J. Rasmussen, K. Saeki, and V. A. Turikov, "Observations of solitary structures in a magnetized, plasma loaded waveguide," *Physica Scripta* **20**, 328–335 (1979), <https://doi.org/10.1088/0031-8949/20/3-4/005>.
- ²⁹K. Saeki, P. Michelsen, H. L. Pécseli, and J. J. Rasmussen, "Formation and coalescence of electron solitary holes," *Phys. Rev. Lett.* **42**, 501–504 (1979), <https://doi.org/10.1103/PhysRevLett.42.501>.
- ³⁰J. R. Danielson, F. Andereg, and C. F. Driscoll, "Measurement of landau damping and the evolution to a bgk equilibrium," *Phys. Rev. Lett.* **92**, 245003 (2004), <https://doi.org/10.1103/PhysRevLett.92.245003>.
- ³¹M. Temerin, K. Cerny, W. Lotko, and F. S. Mozer, "Observations of double layers and solitary waves in the auroral plasma," *Phys. Rev. Lett.* **48**, 1175–1179 (1982), <https://doi.org/10.1103/PhysRevLett.48.1175>.
- ³²R. Bostrom, G. Gustafsson, B. Holback, G. Holmgren, H. Koskinen, and P. Kintner, "Characteristics of solitary waves and weak double layers in the magnetospheric plasma," *Phys. Rev. Lett.* **61**, 82–85 (1988), <https://doi.org/10.1103/PhysRevLett.61.82>.
- ³³A. Mikkilä, H. Koskinen, R. Bostrom, and B. Holback, "On theories attempting to explain observations of solitary waves and weak double layers in the auroral magnetosphere," *Physica Scripta* **39**, 787–793 (1989), <https://doi.org/10.1088/0031-8949/39/6/023>.
- ³⁴H. Matsumoto, H. Kojima, T. Miyatake, Y. Omura, M. Okada, I. Nagano, and M. Tsutsui, "Electrostatic solitary waves (esw) in the magnetotail: Ben wave forms observed by geotail," *Geophysical Research Letters* **21**, 2915–2918 (1994), <https://agupubs.onlinelibrary.wiley.com/doi/pdf/10.1029/94GL01284>.
- ³⁵H. Kojima, H. Matsumoto, S. Chikuba, S. Horiyama, M. Ashour-Abdalla, and R. R. Anderson, "Geotail waveform observations of broadband/narrowband electrostatic noise in the distant tail," *Journal of Geophysical Research: Space Physics* **102**, 14439–14455 (1997), <https://agupubs.onlinelibrary.wiley.com/doi/pdf/10.1029/97JA00684>.
- ³⁶F. S. Mozer, R. E. Ergun, M. Temerin, C. Cattell, J. Dombeck, and J. Wygant, "New features of time domain electric-field structures in the auroral acceleration region," *Phys. Rev. Lett.* **79**, 1281–1284 (1997), <https://doi.org/10.1103/PhysRevLett.79.1281>.
- ³⁷S. D. Bale, P. J. Kellogg, D. E. Larsen, R. P. Lin, K. Goetz, and R. P. Lepping, "Bipolar electrostatic structures in the shock transition region: Evidence of electron phase space holes," *Geophysical Research Letters* **25**, 2929–2932 (1998), <https://agupubs.onlinelibrary.wiley.com/doi/pdf/10.1029/98GL02111>.
- ³⁸L. Muschietti, R. E. Ergun, I. Roth, and C. W. Carlson, "Phase-space electron holes along magnetic field lines," *Geophysical Research Letters* **26**, 1093–1096 (1999),

- <https://agupubs.onlinelibrary.wiley.com/doi/pdf/10.1029/1999GL90020p>, pp. 231–247, https://doi.org/10.1007/978-1-4899-7413-6_9.
- ³⁹K. V. Roberts and H. L. Berk, “Nonlinear evolution of a two-stream instability,” *Phys. Rev. Lett.* **19**, 297–300 (1967), <https://doi.org/10.1103/PhysRevLett.19.297>.
 - ⁴⁰R. L. Morse and C. W. Nielson, “Numerical simulation of warm two-beam plasma,” *The Physics of Fluids* **12**, 2418–2425 (1969), <https://aip.scitation.org/doi/pdf/10.1063/1.1692361>.
 - ⁴¹R. L. Morse and C. W. Nielson, “One-, two-, and three-dimensional numerical simulation of two-beam plasmas,” *Phys. Rev. Lett.* **23**, 1087–1090 (1969), <https://doi.org/10.1103/PhysRevLett.23.1087>.
 - ⁴²H. L. Berk, C. E. Nielsen, and K. V. Roberts, “Phase space hydrodynamics of equivalent nonlinear systems: Experimental and computational observations,” *The Physics of Fluids* **13**, 980–995 (1970), <https://aip.scitation.org/doi/pdf/10.1063/1.1693039>.
 - ⁴³O. Ishihara, A. Hirose, and A. B. Langdon, “Nonlinear evolution of buneman instability,” *The Physics of Fluids* **24**, 452–464 (1981), <https://aip.scitation.org/doi/pdf/10.1063/1.863392>.
 - ⁴⁴A. Ghizzo, B. Izrar, P. Bertrand, E. Fijalkow, M. R. Feix, and M. Shoucri, “Stability of bernsteingreenekruskal plasma equilibria. numerical experiments over a long time,” *The Physics of Fluids* **31**, 72–82 (1988), <https://aip.scitation.org/doi/pdf/10.1063/1.866579>.
 - ⁴⁵H. Schamel, “Stability of electron vortex structures in phase space,” *Phys. Rev. Lett.* **48**, 481–483 (1982), <https://doi.org/10.1103/PhysRevLett.48.481>.
 - ⁴⁶Y. Omura, H. Matsumoto, T. Miyake, and H. Kojima, “Electron beam instabilities as generation mechanism of electrostatic solitary waves in the magnetotail,” *Journal of Geophysical Research: Space Physics* **101**, 2685–2697 (1996), <https://agupubs.onlinelibrary.wiley.com/doi/pdf/10.1029/95JA03145>.
 - ⁴⁷G. Manfredi, “Long-time behavior of nonlinear landau damping,” *Phys. Rev. Lett.* **79**, 2815–2818 (1997), <https://doi.org/10.1103/PhysRevLett.79.2815>.
 - ⁴⁸P. A. Sweet, “14. the neutral point theory of solar flares,” *Symposium - International Astronomical Union* **6**, 123134 (1958), <https://doi.org/10.1017/S0074180900237704>.
 - ⁴⁹E. N. Parker, “Sweet’s Mechanism for Merging Magnetic Fields in Conducting Fluids,” *Journal of Geophysical Research* **62**, 509–520 (1957), <https://doi.org/10.1029/JZ062i004p00509>.
 - ⁵⁰H. E. Petschek, “Magnetic Field Annihilation,” in *The Physics of Solar Flares, Proceedings of the AAS-NASA Symposium held 28-30 October, 1963 at the Goddard Space Flight Center, Greenbelt, MD. Edited by Wilnot N. Hess. Washington, DC: National Aeronautics and Space Administration, Science and Technical Information Division, 1964., p.425*, Vol. 50 (1964) p. 425.
 - ⁵¹R. B. White, “Resistive reconnection,” *Rev. Mod. Phys.* **58**, 183–207 (1986), <https://doi.org/10.1103/RevModPhys.58.183>.
 - ⁵²J. B. Taylor, “Relaxation and magnetic reconnection in plasmas,” *Rev. Mod. Phys.* **58**, 741–763 (1986), <https://doi.org/10.1103/RevModPhys.58.741>.
 - ⁵³E. R. Priest and T. Forbes, *Magnetic Reconnection: MHD Theory and Applications* (Cambridge Univ. Press, 2000).
 - ⁵⁴D. Biskamp, *Magnetic Reconnection in Plasmas* (Cambridge University Press, 2000).
 - ⁵⁵A. Bhattacharjee, “Impulsive magnetic reconnection in the earth’s magnetotail and the solar corona,” *Annual Review of Astronomy and Astrophysics* **42**, 365–384 (2004), <https://doi.org/10.1146/annurev.astro.42.053102.134039>.
 - ⁵⁶J. Birn and E. R. Priest, *Reconnection of magnetic fields: magnetohydrodynamics and collisionless theory and observations* (Cambridge University Press, 2007).
 - ⁵⁷M. Yamada, R. Kulsrud, and H. Ji, “Magnetic reconnection,” *Rev. Mod. Phys.* **82**, 603–664 (2010), <https://doi.org/10.1103/RevModPhys.82.603>.
 - ⁵⁸H. Karimabadi, V. Roytershteyn, W. Daughton, and Y.-H. Liu, “Recent evolution in the theory of magnetic reconnection and its connection with turbulence,” in *Microphysics of Cosmic Plasmas*, edited by A. Balogh, A. Bykov, P. Cargill, R. Dendy, T. Dudok de Wit, and J. Raymond (Springer US, Boston, MA, 2014).
 - ⁵⁹A. Lazarian, G. L. Eyink, E. T. Vishniac, and G. Kowal, “Magnetic reconnection in astrophysical environments,” in *Magnetic Fields in Diffuse Media*, edited by A. Lazarian, E. M. de Gouveia Dal Pino, and C. Melioli (Springer Berlin Heidelberg, Berlin, Heidelberg, 2015) pp. 311–372, https://doi.org/10.1007/978-3-662-44625-6_12.
 - ⁶⁰M. Hesse, N. Aunai, J. Birn, P. Cassak, R. E. Denton, J. F. Drake, T. Gombosi, M. Hoshino, W. Matthaeus, D. Sibeck, and S. Zenitani, “Theory and modeling for the magnetospheric multiscale mission,” *Space Science Reviews* **199**, 577–630 (2016), <https://doi.org/10.1007/s11214-014-0078-y>.
 - ⁶¹M. L. Goldstein, M. Ashour-Abdalla, A. F. Viñas, J. Dorelli, D. Wendel, A. Klimas, K.-J. Hwang, M. El-Alaoui, R. J. Walker, Q. Pan, and H. Liang, “Mission oriented support and theory (most) for mms—the goddard space flight center/university of california los angeles interdisciplinary science program,” *Space Science Reviews* **199**, 689–719 (2016), <https://doi.org/10.1007/s11214-014-0127-6>.
 - ⁶²J. F. Drake, M. Swisdak, C. Cattell, M. A. Shay, B. N. Rogers, and A. Zeiler, “Formation of electron holes and particle energization during magnetic reconnection,” *Science* **299**, 873–877 (2003), <https://science.sciencemag.org/content/299/5608/873.full.pdf>.
 - ⁶³W. Daughton, J. Scudder, and H. Karimabadi, “Fully kinetic simulations of undriven magnetic reconnection with open boundary conditions,” *Physics of Plasmas* **13**, 072101 (2006), <https://doi.org/10.1063/1.2218817>.
 - ⁶⁴K. Fujimoto and S. Machida, “A generation mechanism of electrostatic waves and subsequent electron heating in the plasma sheetlobe boundary region during magnetic reconnection,” *Journal of Geophysical Research: Space Physics* **111** (2006), 10.1029/2005JA011542, <https://agupubs.onlinelibrary.wiley.com/doi/pdf/10.1029/2005JA011542>.
 - ⁶⁵H. Che, J. F. Drake, M. Swisdak, and P. H. Yoon, “Electron holes and heating in the reconnection dissipation region,” *Geophysical Research Letters* **37** (2010), 10.1029/2010GL043608, <https://agupubs.onlinelibrary.wiley.com/doi/pdf/10.1029/2010GL043608>.
 - ⁶⁶L.-J. Chen, W. S. Daughton, B. Lefebvre, and R. B. Torbert, “The inversion layer of electric fields and electron phase-space-hole structure during two-dimensional collisionless magnetic reconnection,” *Physics of Plasmas* **18**, 012904 (2011), <https://doi.org/10.1063/1.3529365>.
 - ⁶⁷J. Ng, J. Egedal, A. Le, W. Daughton, and L.-J. Chen, “Kinetic structure of the electron diffusion region in antiparallel magnetic reconnection,” *Phys. Rev. Lett.* **106**, 065002 (2011), <https://doi.org/10.1103/PhysRevLett.106.065002>.
 - ⁶⁸J. Ng, J. Egedal, A. Le, and W. Daughton, “Phase space structure of the electron diffusion region in reconnection with weak guide fields,” *Physics of Plasmas* **19**, 112108 (2012), <https://doi.org/10.1063/1.4766895>.
 - ⁶⁹C. Huang, Q. Lu, H. Zhang, M. Wu, Q. Dong, S. Lu, and S. Wang, “Kinetic simulations of the structures of magnetic island in multiple x line guide field reconnection,” *Physics of Plasmas* **19**, 042111 (2012), <https://doi.org/10.1063/1.4704799>.
 - ⁷⁰S. Y. Huang, M. Zhou, Z. G. Yuan, X. H. Deng, F. Sahraoui, Y. Pang, and S. Fu, “Kinetic simulations of electric field structure within magnetic island during magnetic reconnection and their applications to the satellite observations,” *Journal of Geophysical Research: Space Physics* **119**, 7402–7412 (2014), <https://agupubs.onlinelibrary.wiley.com/doi/pdf/10.1002/2014JA020054>.
 - ⁷¹M. V. Goldman, D. L. Newman, G. Lapenta, L. Anderson, J. T. Gosling, S. Eriksson, S. Markidis, J. P. Eastwood, and R. Ergun, “Čerenkov emission of quasiparallel whistlers by fast electron phase-space holes during magnetic reconnection,” *Phys. Rev. Lett.* **112**, 145002 (2014), <https://doi.org/10.1103/PhysRevLett.112.145002>.
 - ⁷²W. Daughton, V. Roytershteyn, H. Karimabadi, L. Yin, B. Albright, B. Bergen, and K. Bowers, “Role of electron physics in the development of turbulent magnetic reconnection,”

- tion in collisionless plasmas,” *Nature Physics* **7**, 539 (2011), <https://doi.org/10.1038/nphys1965>.
- ⁷³A. Bhattacharjee, Y.-M. Huang, H. Yang, and B. Rogers, “Fast reconnection in high-lundquist-number plasmas due to the plasmoid instability,” *Physics of Plasmas* **16**, 112102 (2009), <https://doi.org/10.1063/1.3264103>.
- ⁷⁴C. S. Ng and S. Ragunathan, “High Lundquist Number Resistive MHD Simulations of Magnetic Reconnection: Searching for Secondary Island Formation,” in *5th International Conference of Numerical Modeling of Space Plasma Flows (ASTRONUM 2010)*, Astronomical Society of the Pacific Conference Series, Vol. 444, edited by N. V. Pogorelov, E. Audit, and G. P. Zank (2011) p. 124, <http://aspbooks.org/publications/444/124.pdf>.
- ⁷⁵Y. S. Ge, J. P. McFadden, J. Raeder, V. Angelopoulos, D. Larson, and O. D. Constantinescu, “Case studies of mirror-mode structures observed by themis in the near-earth tail during substorms,” *Journal of Geophysical Research: Space Physics* **116** (2011), 10.1029/2010JA015546, <https://agupubs.onlinelibrary.wiley.com/doi/pdf/10.1029/2010JA015546>.
- ⁷⁶H. S. Fu, Y. V. Khotyaintsev, A. Vaivads, M. Andr, V. A. Sergeev, S. Y. Huang, E. A. Kronberg, and P. W. Daly, “Pitch angle distribution of suprathermal electrons behind dipolarization fronts: A statistical overview,” *Journal of Geophysical Research: Space Physics* **117** (2012), 10.1029/2012JA018141, <https://agupubs.onlinelibrary.wiley.com/doi/pdf/10.1029/2012JA018141>.
- ⁷⁷M. A. Balikhin, D. G. Sibeck, A. Runov, and S. N. Walker, “Magnetic holes in the vicinity of dipolarization fronts: Mirror or tearing structures?” *Journal of Geophysical Research: Space Physics* **117** (2012), 10.1029/2012JA017552, <https://agupubs.onlinelibrary.wiley.com/doi/pdf/10.1029/2012JA017552>.
- ⁷⁸W. J. Sun, Q. Q. Shi, S. Y. Fu, Z. Y. Pu, M. W. Dunlop, A. P. Walsh, Q. G. Zong, T. Xiao, C. L. Tang, H. Reme, C. Carr, E. Lucek, and A. Fazakerley, “Cluster and tc-1 observation of magnetic holes in the plasma sheet,” *Annales Geophysicae* **30**, 583–595 (2012), <https://doi.org/10.5194/angeo-30-583-2012>.
- ⁷⁹X.-F. Ji, X.-G. Wang, W.-J. Sun, C.-J. Xiao, Q.-Q. Shi, J. Liu, and Z.-Y. Pu, “Emhd theory and observations of electron solitary waves in magnetotail plasmas,” *Journal of Geophysical Research: Space Physics* **119**, 4281–4289 (2014), <https://agupubs.onlinelibrary.wiley.com/doi/pdf/10.1002/2014JA019924>.
- ⁸⁰T. Sundberg, D. Burgess, and C. T. Haynes, “Properties and origin of subproton-scale magnetic holes in the terrestrial plasma sheet,” *Journal of Geophysical Research: Space Physics* **120**, 2600–2615 (2015), <https://agupubs.onlinelibrary.wiley.com/doi/pdf/10.1002/2014JA020856>.
- ⁸¹Z. Zhima, J. Cao, H. Fu, W. Liu, L. Chen, M. Dunlop, X. M. Zhang, and X. H. Shen, “Whistler mode wave generation at the edges of a magnetic dip,” *Journal of Geophysical Research: Space Physics* **120**, 2469–2476 (2015), <https://agupubs.onlinelibrary.wiley.com/doi/pdf/10.1002/2014JA020786>.
- ⁸²D. J. Gershman, J. C. Dorelli, A. F. Vias, L. A. Avanov, U. Gliese, A. C. Barrie, V. Coffey, M. Chandler, C. Dickson, E. A. MacDonald, C. Salo, M. Holland, Y. Saito, K.-A. Sauvaud, B. Lavraud, W. R. Paterson, R. Torbert, L.-J. Chen, K. Goodrich, C. T. Russell, R. J. Strangeway, B. L. Giles, C. J. Pollock, T. E. Moore, and J. L. Burch, “Electron dynamics in a subproton-gyroscale magnetic hole,” *Geophysical Research Letters* **43**, 4112–4118 (2016), <https://agupubs.onlinelibrary.wiley.com/doi/pdf/10.1002/2016GL068545>.
- ⁸³K. A. Goodrich, R. E. Ergun, F. D. Wilder, J. Burch, R. Torbert, Y. Khotyaintsev, P.-A. Lindqvist, C. Russell, R. Strangeway, W. Magnes, D. Gershman, B. Giles, R. Nakamura, J. Stawarz, J. Holmes, A. Sturner, and D. M. Malaspina, “Mms multipoint electric field observations of small-scale magnetic holes,” *Geophysical Research Letters* **43**, 5953–5959 (2016), <https://agupubs.onlinelibrary.wiley.com/doi/pdf/10.1002/2016GL069157>.
- ⁸⁴C. S. Ng and H. Tang, “Kinetic Flux Rope Solutions for Realistic Electron/Ion Temperature Ratios,” in *AGU Fall Meeting Abstracts*, Vol. 2018 (2018) pp. SM13B–2870, <https://ui.adsabs.harvard.edu/abs/2018AGUFMSM13B2870N>.